

Surface Degradation and Chemical Electrolyte Oxidation Induced by the Oxygen Released from Layered Oxide Cathodes in Li–Ion Batteries

Daniela Leanza,^[a] Marta Mirolo,^[a, b] Carlos A. F. Vaz,^[b] Petr Novák,^[a] and Mario El Kazzi^{*[a]}

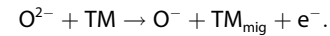
High-resolution, surface sensitive soft X-ray photoemission electron microscopy (XPEEM) reveals the fine interplay between oxygen and transition metal (TM) redox activities on the surface of a $\text{Li}_{1.17}(\text{Ni}_{0.22}\text{Co}_{0.12}\text{Mn}_{0.66})_{0.83}\text{O}_2$ (Li-rich NCM) electrode. We demonstrate that the oxidation of oxygen in the lattice is accompanied by TM reduction already at 4.47 V vs. Li^+/Li , as a result of oxygen loss from the surface, the latter process being enhanced at 4.8 V where oxygen gas reaches a maximum release rate. Simultaneously, we find evidence for the chemical

oxidation of the electrolyte solvents above 4.8 V induced by the released oxygen, leading to the formation of a carbonate by-products layer that covers homogeneously the particles of the counter electrode $\text{Li}_4\text{Ti}_5\text{O}_{12}$ (LTO). The latter observation demonstrates that migration-diffusion of such oxidized solvent by-products occurs only when the solvents are chemically oxidized. We showed also that the Li-rich NCM is susceptible to oxygen loss during soaking in the electrolyte, which causes TMs reduction and the poisoning of the counter electrode.

1. Introduction

The contemporary trend towards a sustainable and energy-efficient infrastructure follows in the direction of coupling renewable energy resources with electrochemical energy storage, preferably based on Li-ion battery technology. From the storage perspective, batteries based on positive materials having an excess of Li-ions hosted in a layered oxide, such as Li-rich $\text{Li}_{1.17}(\text{Ni}_{0.22}\text{Co}_{0.12}\text{Mn}_{0.66})_{0.83}\text{O}_2$ (Li-rich NCM), hold the promise for the highest practical energy density and cost balance.^[1] The higher energy density content arises from the combination of the enhanced reversible specific charge (> 250 mAh/g) and higher working potential (> 4.7 V vs. Li^+/Li) compared to the conventional stoichiometric NCM-materials (e.g. $\text{LiNi}_{0.33}\text{Co}_{0.33}\text{Mn}_{0.33}\text{O}_2$, NCM111). Such exceptional electrochemical performance is achieved when coupling cationic redox activity (from the transition metals Mn, Co and Ni) and anionic redox couple (arising from oxygen O^{2-}), which gives rise to a characteristic stair-case potential curve during the first charge (delithiation). Indeed, at the onset of charge the removal of Li-ions is balanced with the oxidation of the transition metals (TMs) (i.e. Co^{3+} to Co^{4+} and Ni^{2+} to Ni^{4+}) giving rise to the first sloping plateau. At potentials higher than 4.5 V vs. Li^+/Li , the charge balancing is fulfilled by the oxygen anions, accounting for the long activation plateau characteristic for this class of Li-rich

layered oxides. Such plateau appears only at the first charge and is reported to be induced by the reversible $2\text{O}^{2-}/\text{O}_2^{n-}$ -process and an irreversible loss of lattice O^{2-} . The latter is stated to be at the origin of a series of surface reactions and irreversible structural changes.^[2,3] Establishing the role of cationic and anionic redox couples in such materials has been a topic of intense debate and controversy. Tarascon *et al.* have first suggested that oxidation of oxygen generally results in the pairing of oxygen ions, leading to an effective $2\text{O}^{2-}/\text{O}_2^{n-}$ redox couple, which is stabilized against oxygen gas evolution due to the presence of 4d and 5d TMs.^[3–5] Recently, they also proved that a $n\text{O}^{2-}/\text{O}^{n-}$ couple is reversibly oxidized (on charge) and reduced (on discharge) in the bulk of a 3d TMs-based material (i.e. Li-rich NCM), by monitoring the O1s core level evolution using X-ray photoelectron spectroscopy (XPS).^[3,6] On a similar oxide, Bruce and coworkers^[7,8] proposed instead a localized hole $\text{O}^{2-}/\text{O}^{-}$ mechanism based on O K-edge absorption spectroscopy (XAS) and resonant inelastic X-ray scattering (RIXS). A strong correlation between TMs and O redox has been instead confirmed by Gent *et al.*,^[9] who interpret the oxidation of oxygen $\text{O}^{2-} \rightarrow \text{O}^- + \text{e}^-$ not as a static process but rather as a dynamic structure-redox coupling, described with a concomitant migration of the TMs:



Regardless of the mechanism that the O^{2-} anions follow in the redox process, we are interested here in the role that oxygen redox activity can have on the electrolyte stability and on the surface structure integrity of NCM-based cathodes. It is important to point out that the electrochemical signature of oxygen redox activity is often coupled with the irreversible process of oxygen gas formation that inevitably triggers a structural modification commonly associated with a spinel and

[a] Dr. D. Leanza, M. Mirolo, Prof. Dr. P. Novák, Dr. M. El Kazzi
Electrochemistry Laboratory, Paul Scherrer Institute
CH-5232 Villigen PSI, Switzerland
E-mail: mario.el-kazzi@psi.ch

[b] M. Mirolo, Dr. C. A. F. Vaz
Swiss Light Source, Paul Scherrer Institute
CH-5232 Villigen PSI, Switzerland

 Supporting information for this article is available on the WWW under <https://doi.org/10.1002/batt.201800126>

 An invited contribution to a Special Issue on SEI and Interphases at Electrodes

rock-salt-like structure and containing TMs in a reduced valence state.^[10–12]

On the other hand, the oxygen loss from the layered oxide not only has an impact on the surface structure, but can also undermine the stability of the electrolyte. In recent reports, it has been demonstrated that chemical oxidation of the carbonate solvents, such as ethylene and dimethyl carbonate (EC and DMC, respectively), initiated by the oxygen is indeed thermodynamically favorable and such decomposition could be the major reason why high-potential cells generate gases and have poor capacity retention.^[13,14] The oxygen gas is usually detected via differential electrochemical mass spectrometry (DEMS) at a potential of about 4.7 V vs. Li⁺/Li, accompanied with prominent CO₂ gas evolution.^[14–17] Also earlier O₂ and CO₂ evolution signals have been reported along the long plateau (between 4.3 V and 4.4 V vs. Li⁺/Li), as an effect of the oxygen redox activity^[7] and/or Ni content in the structure (i.e. the higher the Ni content, the earlier/faster the onset potential of O₂ release).^[18] Concerning the CO₂ gas, which shows usually a continuous evolution with the delithiation of the NCM cathode, there is an agreement that its early origin stems from the Li₂CO₃ decomposition at potentials below 4.4 V, the latter being a common residue from the synthesis route and ageing due to air exposure. There are however two interpretations of the CO₂ evolution above 4.4 V. Some reports^[15,19] suggest that the Li₂CO₃ continues to decompose at high potentials, while others^[7,14,18] ascribe the CO₂ formation to a chemical reaction between the oxygen lattice and the electrolyte. Beside the chemical-triggered reactions, the CO₂ gas can be also the main side reaction product of the electrochemically-induced electrolyte decomposition. Even though carbonate-based solvents have a theoretical oxidation potential of ~6.0 V vs. Li⁺/Li^[13,20,21], experimental studies show that they can be already electrochemically oxidized in the range from 4.5–6.5 V.^[22,23]

These manifold chemical and electrochemical reactions that can occur at high-potential represent a big hurdle towards the successful commercialization of the Li-rich NCM electrodes, making urgent and critical their complete understanding in order to take full advantage of their total specific charge. Given the heterogeneous nature of such processes with respect to the different particles composing the electrodes and the need to follow the electrochemical behavior at the level of individual components, we employ X-ray photoemission electron microscopy (XPEEM) as a high lateral resolution technique (better than 70 nm) and high surface sensitivity (below 3 nm). In our previous work^[28] performed on early and long cycled Li-rich NCM, we (i) validated XPEEM as suitable technique to investigate the electrodes' complex surface reactivity at the interface with the electrolyte and (ii) demonstrated the instability of the TMs, binder and electrolyte at high voltage and their direct impact on the surface of the counter electrode. Here, we complement the previous work by examining particularly the role and the impact of the released oxygen from the surface of the active materials on the degradation of the electrode-electrolyte interface. Specifically, we investigated the early stages of cycling of Li-rich NCM material as positive electrode and aimed at understanding, by surface-sensitive X-

ray absorption spectroscopy (XAS) analysis, how oxygen activity can influence (i) the surface electronic structure evolution of anionic and cationic couples by following the O K-edge and Mn, Co and Ni L-edges and (ii) the electrolyte stability towards oxidation by monitoring the evolution of the C K-edge. This spectroscopic study is carried out at individual secondary and primary particles of Li-rich NCM and carbon, since their size fall in the same range as the XPEEM lateral resolution. We will also examine the impact of the processes (i) and (ii) on the negative electrode Li₄Ti₅O₁₂ (LTO) by following the evolution of the C K-edge, on both carbon and LTO particles. In doing so, we conduct a detailed analysis along different states of charge (SoC) of the first delithiation of the Li-rich NCM cycled vs. LTO and we compare the results with the stoichiometric NCM111 also cycled vs. LTO, where the oxygen release is about 8 times lower.^[17] Finally we will discuss the surface evolution of LTO when cycled vs. LiNi_{0.5}Mn_{1.5}O₄ (LNMO), where the oxygen evolution is practically negligible.^[24]

2. Results

2.1. Electrochemical Cycling

The potential profile recorded in a 3-electrode cell configuration for the first charge of Li-rich NCM (blue) cycled vs. LTO (red) is shown in Figure 1. The potential profiles of NCM111 and LNMO cycled vs. LTO are presented in Figure S1 in the Supplementary Information. The potential values examined in this study for both cathodes and the LTO anode are marked with circles and considered along the first delithiation process.

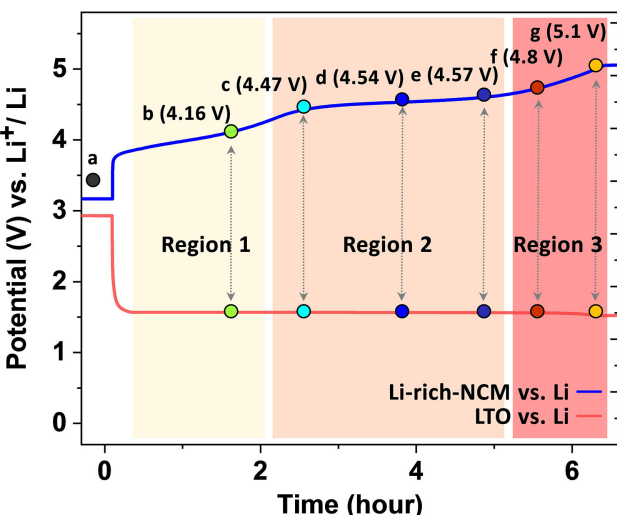


Figure 1. Potential profile for the 1st delithiation of the Li-rich NCM (blue) cycled vs. LTO (red) in a 3-electrode cell using metallic lithium as reference and a C/5 cycling rate in LP30 electrolyte. The first delithiation is characterized by a staircase-like profile. The potential values examined in this study are marked with colored circles. During the first plateau (Region 1) only cationic couples (Co and Ni) are involved in the charge compensation upon lithium ion removal. On the second plateau (Region 2) the charge compensation is fulfilled with oxidation of oxygen. The Region 3 is considered at the end of the charge after O₂ is released from the cathode.

During the first delithiation (oxidation) of the Li-rich NCM, three regions have been considered based on the redox processes of Li-rich NCM. *Region 1* extends until 4.4 V and is associated with the oxidation of Ni^{2+} and Co^{3+} to Ni^{4+} and Co^{4+} (cationic couples), respectively.^[25] *Region 2* is the second plateau, approximately until 4.6 V, where bulk oxygen is oxidized $\text{O}^{2-} \rightarrow \text{O}^{\cdot-} + \text{e}^-$ (anionic couple). *Region 3* refers to the sloping region until the end of the charge at 5.1 V, where CO_2 and O_2 gas formation is detected. A similar study has been carried out also on NCM111 at various potentials across the first delithiation. Finally, the LTO anode is also examined at the end of the first charge at 5 V against LNMO. For a complete list of the potential values considered for each cathode, we refer to Table S1 in the Supplementary Information. All the potentials reported in the manuscript are referred vs. Li^+/Li .

2.2. Cathode Surface Modification at Open Circuit Potential (OCP)

Before starting the investigation of the cycled electrodes, we examined the chemical surface evolution of the Li-rich NCM and NCM111 cathodes at open circuit potential (OCP). We notice that, after soaking in LP30 for only 8 hours, the surface

of the Li-rich NCM particles contain already reduced TMs (Figure 2, blue spectra) and their amount increases with soaking time (54 days) (Figure 2, gold spectra). This behavior is noticeable by the strong features that increase in amplitude at low photon energy of the Mn (between 642 eV and 640 eV) and Co (at 779 eV) L_3 -edges associated with the presence of $\text{Mn}^{2+/-3+}$ and Co^{2+} respectively, while Ni remains in +2 oxidation state. Additionally, we notice that the reduced TMs are more homogeneously distributed among the electrode particles after long exposure with the electrolyte. Thanks to the high lateral resolution of XPEEM, we can indeed easily visualize how the reduced TMs are spatially distributed within the particle surface, by following the evolution of a specific absorption edge along a desired zone of interest of the cathode. For example, the distribution of the Co^{2+} at the Co L_3 -edge (taken at 779 eV) can be clearly seen in Figure 2a and 2d, where a XPEEM elemental map is color-coded according to the legend on the left of the images. The red color indicating particles with high amount of Co in oxidation state (+2) and the blue color corresponding to particles with a less reduced Co. The more uniform magenta color after 54 days of OCP corresponds to the homogeneous presence of reduced TMs, as compared to the one after 8 hours. The reason for such drastic surface changes can be related either to (i) the loss Li-ions that are in contact with the

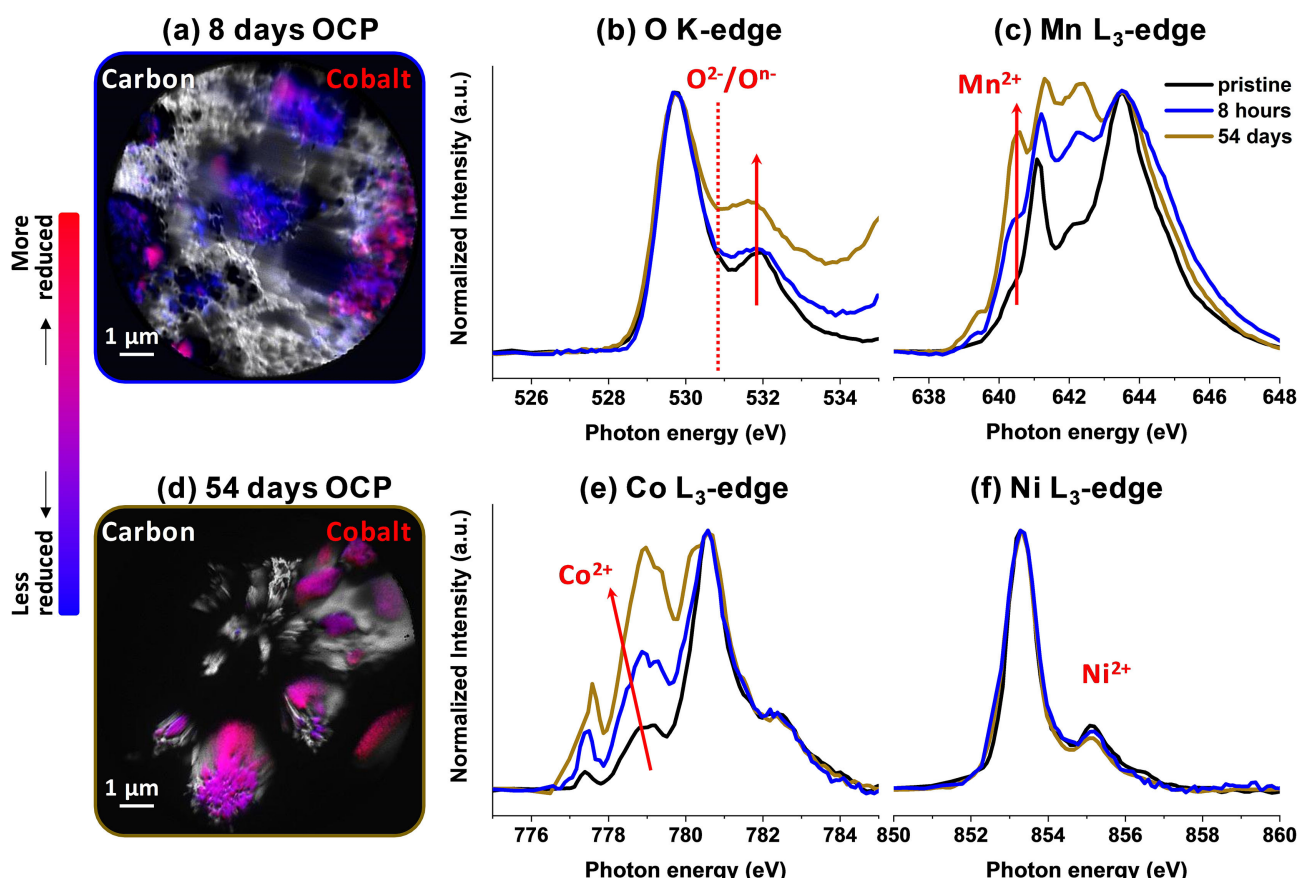


Figure 2. Reconstructed XPEEM chemical maps of the Li-rich NCM electrode kept at OCP for (a) 8 hours and (d) 54 days in LP30 electrolyte. The grey color corresponds to carbon particles taken at the C K-edge (285.6 eV), whereas the blue and red correspond to the Li-rich NCM particles taken at two different oxidation states of Co L-edge (781 eV- Co^{3+}) and (779 eV- Co^{2+}), respectively. Local XAS taken on the more reduced areas of Li-rich NCM at the (b) O K-edge, (c) Mn, (e) Co and (f) Ni L_3 -edges compared to the pristine electrode.

electrolyte (which implicitly means the oxidation of the electrolyte at a low rate), and that can lead to a surface reorganization with reduced TMs and a possible formation of carbonate-rich layer^[26,27] or (ii) to the oxygen lattice surface reactivity, induced by the possible presence of HF in the electrolyte, that cause etching of the oxide particles. In this regard, the disappearance of the adventitious carbonate layer (present in the pristine electrode) already after 8 hours of OCP allow us to exclude the former reaction (see Figure S2 in the Supplementary Information). Also, we do not detect traces of a passivating by-products layer after long exposure neither on carbon nor on Li-rich particles. On the other hand, the layer of reduced TMs is unstable at OCP and tends to dissolve in the electrolyte, as confirmed via the deposition of Mn, Co and Ni on the surface of LTO after 54 days of soaking in LP30 (Figure S3, Supporting information). The clusters-like morphology and the valence states of the TMs on the LTO anode are in accordance to our previous results.^[28] Changing the cathode stoichiometry to an equal ratio of the TMs, as in the case of NCM111, does not alter the behavior at OCP, as discussed for the Li-rich NCM (Figure S4, Supplementary information).

2.3. TMs Electronic Structure Changes along the First Delithiation and Impact of Oxygen Release

Region 1 (First plateau before the oxygen oxidation): Figure 3a, b, c and d show local XAS spectra acquired on Li-rich NCM

particles at the O K-edge and Mn, Co and Ni L₃-edges, respectively. They are performed on pristine (black) and delithiated electrode at 4.16 V vs. Li⁺/Li (green). We can clearly notice that across *Region 1*, Ni²⁺ is oxidized to Ni⁴⁺ together with Co³⁺ to Co⁴⁺. This behavior is identified by the strong Ni L₃-edge feature evolution at 855 eV and the shift to higher photon energy of the Co L₃-edge accompanied by a broadening of the feature at 782.4 eV. These variations correlate with the broadening of the O-peaks at 528.8 eV and 531.9 eV, highlighted by the blue arrows, as a result of the progressive depopulation of the hybridized states O_{2p}-TM_{3d}.^[29] As reported recently,^[7,9] the O K-edge can be used also to track the "O-redox" in the bulk of the particles, by monitoring the evolution of the component at 530.8 eV. Such observation is more straightforward when using transmission XAS methods that probe the bulk of the material. In our method, the partial electron yield limits our detection to ca. 3 nm from the surface of the active material particles, meaning that the sensitivity towards the "O-redox" is practically not relevant and the changes at the O K-edge mainly correlate with the TMs redox. With regards to the valence state of the TMs, it is worth mentioning that at 4.16 V neither nickel nor cobalt are in a full oxidation state of +4 and they are not homogeneously distributed across the cathode (not all the particles are delithiated). Additionally, the non-delithiated particles (according to the TMs oxidation state) show reduced TMs on their surface. The former observation is associated with the partial delithiation of the cathode, as the cell is stopped in the middle

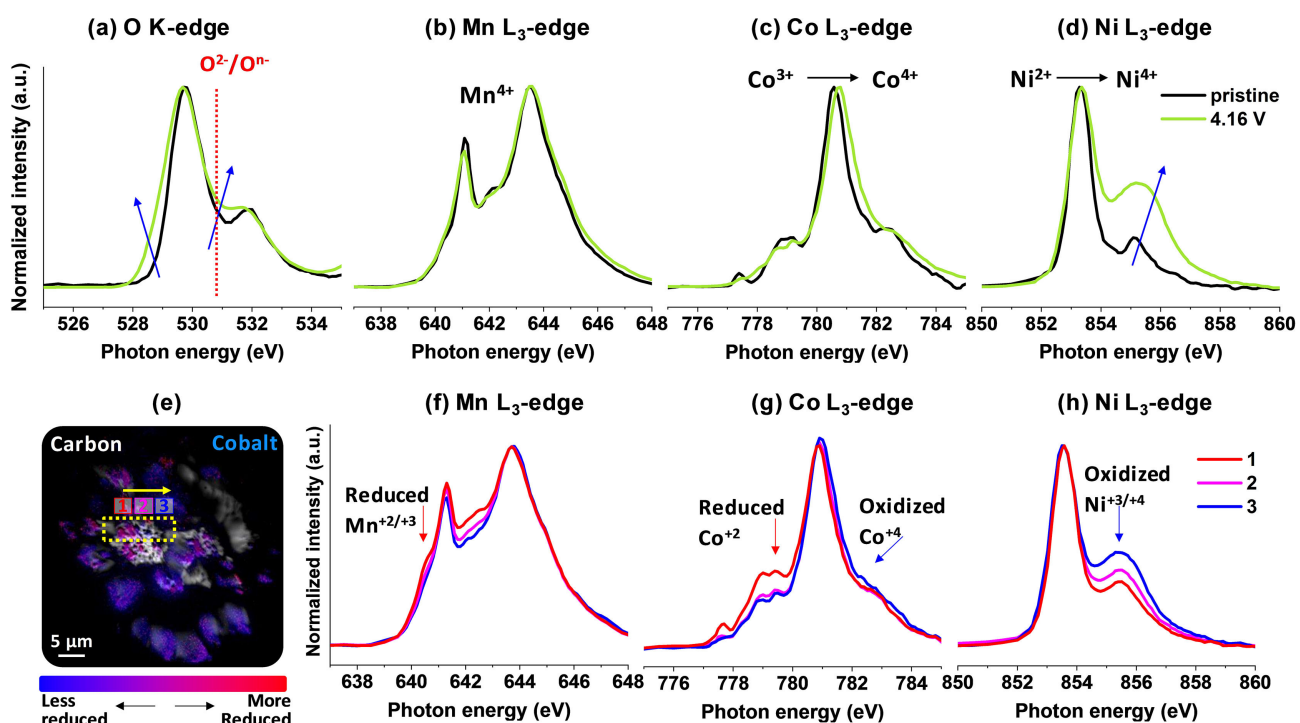


Figure 3. Local XAS at the (a) O K-edge, (b) Mn, (c) Co and (d) Ni L₃-edges acquired on a delithiated Li-rich NCM particle at 4.16 V (green) and compared to the pristine electrode (black). (e) XPEEM chemical map carried out on Li-rich-NCM particles at the C K-edge (grey) and Co L₃-edge (blue) for the cycled cathode at 4.16 V. The color gradient on the map is due to inhomogeneity in the oxidation state of the TMs within secondary particles of the active material, showing the less reduced (blue) and the more reduced (magenta/red) parts of the cathode. XAS along 1 (more reduced), 2 (intermediate) and 3 (more oxidized) regions taken at the (f) Mn, (g) Co and (h) Ni L₃-edges.

of the first potential plateau. The latter aspect is related to the remaining reduced TMs caused by the surface reaction at OCP, as described above.

The elemental contrast image at a primary particle of the Li-rich NCM in Figure 3e confirms our observation. The variations of the absorption edges in three different zones highlighted with a yellow square show again differences in oxidation state at the Co L₃-edge. Here, the XPEEM elemental map is color-coded, with the red color indicating a lower Co oxidation state (+2) from the spectral feature of 779 eV and the blue color less reduced Co. The same trend is also observed at the absorption energy of manganese and nickel and as shown in Figure S5, in the Supplementary Information. The Mn, Co and Ni L₃-edges probed in a 10 μm region of a secondary Li-rich NCM particle are shown in Figure 3f–g–h and show that they are all more reduced in the area 1 (red curves) compared to area 3 (blue curves). The spectra acquired on the particles along the surface show that the electrochemically delithiated particles do not contain reduced TMs, whereas the non-delithiated particles do. In our experiment, the OCP period of 6 hours preceding the galvanostatic cycling can explain the presence of reduced TMs on the non-delithiated particles at 4.16 V. Those TMs can then be oxidized as soon as Li-ions are removed or, more likely, dissolved into the electrolyte followed by diffusion-migration to the anode, as observed at OCP.

The Li-rich NCM in *Region 1* is compared to NCM111 cycled at 4.11 V, a potential where both Co and Ni are supposed to be in a full oxidation state of +4 (see NCM111 cyclic voltammetry

curve in Figure S6, Supplementary Information) and where oxygen redox activity or gas evolution is not expected.^[30,31] The local XAS on NCM111 confirm the presence of Co⁴⁺ and Ni⁴⁺, as attested by the shift to higher photon energy of the Co L₃-edge and the rapid increase of the high-energy peak in the Ni L₃-edge at 855 eV (Figure S7, Supplementary Information). The absorption feature at 855 eV, characteristic for the oxidized Ni⁴⁺, is considerably more pronounced in comparison to the Li-rich NCM at 4.16 V. This behavior is not surprising since at 4.16 V the Li-rich NCM does not reach the full oxidation of the TMs as for NCM111. Accordingly, the O K-edge features increase at both 529.7 eV and 531.9 eV following the trend of the Ni and Co L₃-edges. Conversely, although the manganese is not expected to take part in the oxidation process, it shows an apparent reduction feature at 640.3 eV. As explained by Assat *et al.*^[6] this change can be either due to the redox activity of the neighboring Ni and Co and/or to a local crystal structural change. It is important to emphasize here that the surface (electro-) chemical behavior of the NCM111 is similar to that of the Li-rich NCM, showing the disappearance of the reduced TMs (generated at OCP), due to either their electrochemical oxidation (i.e. delithiation) or dissolution in the electrolyte.

Region 2 (second plateau, oxygen oxidation): Upon charging across the second plateau in *Region 2*, we observe no further oxidation of the Li-rich NCM particles (Figure 4). Only at the beginning of the plateau at 4.47 V, where the highest oxidation state of the TMs is expected, the Ni L₃-edge peak at 855 eV increases slightly compared to the one at 4.16 V (added

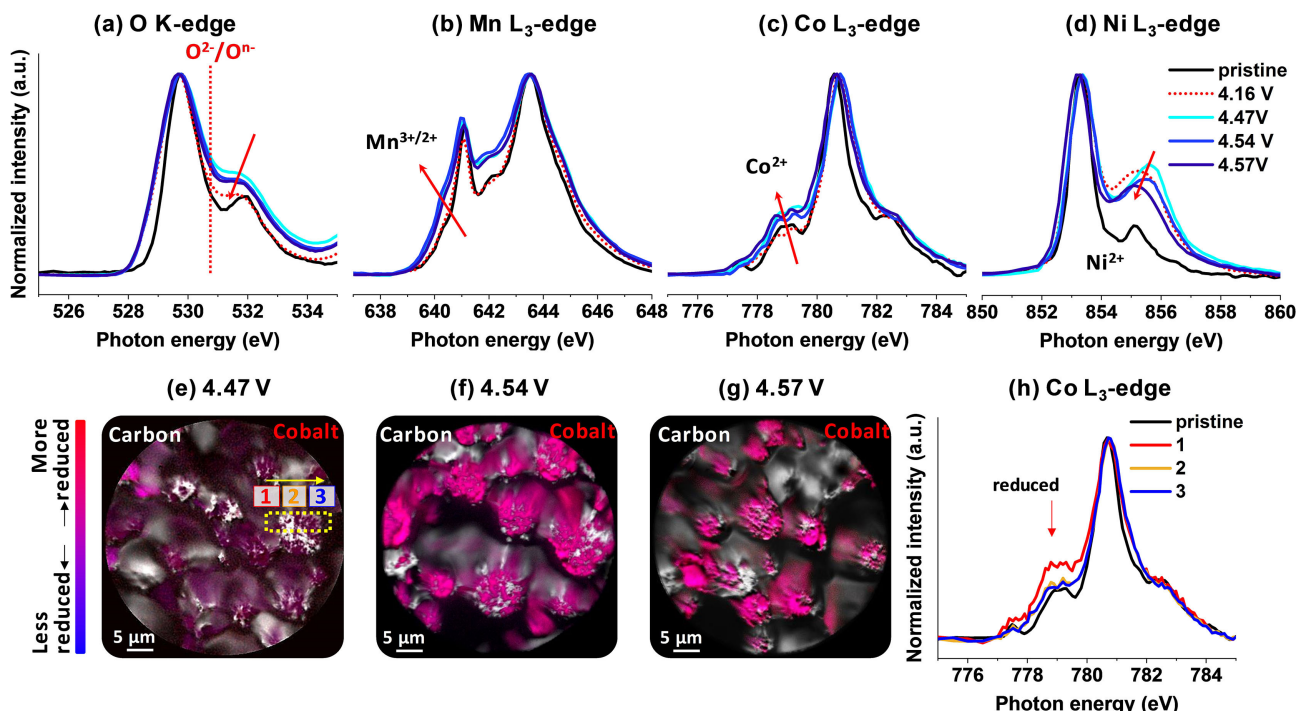


Figure 4. Local XAS at the (a) O K-edge, (b) Mn, (c) Co and (d) Ni L₃-edges acquired on Li-rich-NCM single particle along the second plateau (*Region 2*) from 4.47 V to 4.57 V vs. Li⁺/Li. The potential in *Region 1* at 4.16 V is shown for comparison as dotted green lines. Reconstructed chemical maps carried out on Li-rich-NCM at the C K-edge (grey) and at the Co L₃-edge acquired at 779 eV (in red) for reduced Co and at 781 eV (in blue) for less-reduced Co within the secondary particle of the active material are shown for (e) 4.47 V, (f) 4.54 V and (g) 4.57 V. (h) Local XAS scan at the Co L₃-edge for the particles highlighted in (e) showing the valence distribution.

as dotted lines for reference), but when the charging continues to 4.54 V and 4.57 V, the same peak progressively decreases and shifts towards lower energy together with the main absorption peak at 853.3 eV (Figure 4d). Simultaneously, a gradual increase of the reduced Mn and Co is also observed compared to *Region 1*, as indicated by the rise of the Mn and Co L₃-edges features at low photon energies at 640.3 eV and 778.8 eV, respectively, together with a shift to lower photon energy of the main peak of Co (Figure 4b and 4c). These changes are again consistent with the evolution of the O K-edge (Figure 4a), whose features at 528.8 eV and 531.9 eV, associated with the depopulation of the hybridized states O_{2p}-TM_{3d} remain unchanged.

According to XAS in bulk sensitive mode, a feature at 530.8 eV related to the oxygen redox couple O²⁻/Oⁿ⁻ should increase, as a result of the oxygen oxidation along the second plateau.^[6,7,32] The apparent absence of changes of the "O-redox" component suggests that the oxidized oxygen is unstable at the surface and either reacts immediately with the electrolyte or is released, as O₂ gas, leaving reduced TMs on the cathode surface. Such hypothesis is supported by DEMS measurements which show CO₂ and a slight O₂ gas evolution along the plateau.^[7,17] The mechanism that takes part during this second plateau (*Region 2*), and which leads to the counter-intuitive presence of reduced TMs, is indeed a result of a complex interplay between the concomitant oxidation of the O²⁻/Oⁿ⁻ couple and its loss at the surface. In other words, the reduced TMs on *Region 2* arise from an electrochemical process, in contrast to those observed at OCP, which are generated from a pure chemical interaction with the electrolyte.

In contrast to *Region 1* and to the short-term soaked sample, we observe that the reduced TMs along *Region 2* are more homogeneously distributed across all the Li-rich NCM particles, as observed by the more uniform red/magenta color of the XPEEM images in Figure 4e, f and g, which show, respectively, the contrast images obtained at the C K-edge (grey) and at the Co L₃-edge feature corresponding to more-reduced Co (at 779 eV and displayed in red) and to a less-reduced Co (shown in blue). While at the beginning of the charge (in *Region 1*) the delithiated particles, yielding oxidized TMs, were spatially-separated from the lithiated particles, containing reduced TMs, in *Region 2*, this separation vanishes, since now the particles are more homogeneously delithiated

(supported by the oxidized Co and Ni) and contain simultaneously reduced Mn, Co and Ni, as confirmed by the XAS scan at the Co L-edge in Figure 4h. We attribute this latter behavior to the oxygen loss from the surface. We refer also to the Supplementary Information for the Mn and Ni L-edges scans at 4.47 V in Figure S10 and the local scans at 4.54 V and 4.57 V in Figure S11, which show a similar trend for cobalt.

It is interesting to note that, for NCM111, within the same potential range from 4.3 V to 4.6 V (Figure S7 in the Supplementary Information), there is no signature of reduced TMs. The Co and Ni L₃-edges show evidence for the presence of oxidized Co⁴⁺ and Ni⁴⁺, supported also by the O K-edge feature increases at 529.7 eV. As expected, the Mn L₃-edge does not evolve significantly compared to the 4.11 V. Again, these results highlight the parallelism between O₂ release from the surface and the presence of reduced TMs. The negligible amount of CO₂ and O₂ gas detected from the NCM111 between 4.3 V and 4.6 V^[17,18] agrees with the absence of oxygen oxidation and oxygen loss from the surface. The effect of O₂ on the cathode surface can be observed straightforwardly at the Ni L₃-edge by following the ratio between the main peak at 853 eV and the shoulder at 855 eV. This ratio is almost 1:1 in the case of NCM111 (Figure S7d and 8d, Supplementary Information) and is reduced to almost half for the Li-rich NCM (Figure 4d), highlighting the competing formation of oxidized Ni⁴⁺, driven by the Li-ion removal and the reduced Ni²⁺, as an effect of oxygen loss.

Region 3 (above 4.7 V, after oxygen gas detection): Extending the potential further up to 4.8 V and 5.1 V, located in *Region 3*, strong O₂ and CO₂ gas release are detected on Li-rich NCM on the basis of DEMS measurements.^[7,15,16,19,32,33] In this region, no significant changes are observed for both the O K-edge and the TMs L-edges (Figure 5) as compared to the potential at 4.57 V. Despite the considerable amount of oxygen released, the surface of Li-rich NCM remains covered with a partially oxidized Co and Ni and reduced Mn, Co and Ni. This observation highlights the strong dynamic mechanism that the Li-rich NCM surface experiences at the end of the charge and which combines oxygen loss, TMs reduction and their dissolution in the electrolyte.

The NCM111 cathode is correspondingly cycled at 4.8 V (Figure S9, Supplementary Information), as for *Region 3* on Li-

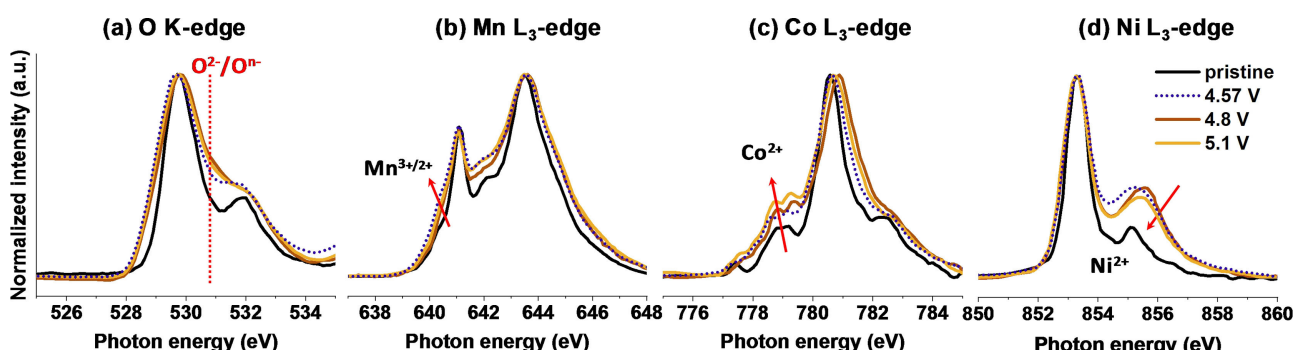


Figure 5. Local XAS at the (a) O K-edge, (b) Mn, (c) Co and (d) Ni L-edges acquired on Li-rich NCM single particle at the end of the 1st delithiation along *Region 3* at 4.8 V (brown) and 5.1 V (yellow). The last potential in *Region 2* at 4.57 V is shown for comparison as dotted blue lines.

rich NCM. At this potential, the NCM111 also releases CO_2 and O_2 gases, caused by the oxygen oxidation, as confirmed by DEMS.^[14,18,30] However, the impact of the oxygen loss seems to be less prominent on the reduction of the TMs as compared to that on the Li-rich NCM, as indicated by the slight decrease of the features at 855 eV and 529.7 eV at the Ni L-edge and at the O K-edge, respectively. This behavior is not surprising, since the amount of gas release is about 8 times smaller than that of the Li-rich cathode.^[17]

2.4. Surface Layer Evolution on Li-rich NCM Cathode

To evaluate the impact of the voltage and oxygen release on the oxidation process of the electrolyte and the possible deposition of electrolyte by-products on the cathode particles, we probed locally the evolution of the C K-edge along the three regions on carbon and Li-rich NCM particles (Figure 6a

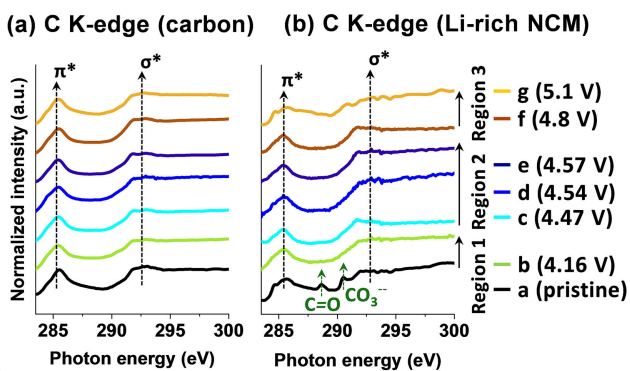


Figure 6. C K-edge acquired locally on (a) conductive carbon and (b) Li-rich NCM particles on pristine electrode (black curves) and across the three regions during the first charge.

and 6b, respectively). It is clear that the cathode is not passivated by a C-containing layer along the charging process on any of its particles, as the C K-edge spectra do not evolve in comparison with the pristine electrode. As we already discussed in a separate publication,^[28] the adventitious carbonate layer that covers only the active material in the pristine state (evidenced by the two small peaks at 288.7 eV and 290.5 eV), decomposes already at 4.16 V in *Region 1*, in agreement with the small amount of CO_2 release always detected by DEMS at the same potential.^[15,19] Similarly, at the NCM111 cathode, no surface by-product layer is detected along the entire charging process (Figure S12, Supplementary Information). The absence of short and long-chain carbonate by-products caused by possible electrochemical and/or chemical oxidation of the electrolyte suggests four likely scenarios: (1) they decompose into volatile by-products (e.g. CO and CO_2); (2) they dissolve into the electrolyte and/or are trapped at the separator surface; (3) they migrate to the counter electrode; or (4) those reactions do not occur. As we show next, the C K-edge evolution on the counter-electrode $\text{Li}_4\text{Ti}_5\text{O}_{12}$ (LTO) provides answers to those questions.

2.5. $\text{Li}_4\text{Ti}_5\text{O}_{12}$ Surface Evolution and Cross-Talk Reaction

Region 1 and Region 2 (below 4.6 V): We already demonstrated in a separate work that the LTO is an appropriate anode to track the possible cross-talk processes with the positive electrode with regard to TMs dissolution and electrolyte by-products species.^[28] Thanks to the high lateral resolution of the XPEEM technique, we proved also in a previous work that the carbonate-based electrolyte reduction can indeed occur on the LTO electrode along the plateau at 1.55 V vs. Li^+/Li via a process that solely involves the particles of LTO active material, whereas the conductive carbon remains free from any detectable surface layer.^[34] Thus, the detection of any surface evolution on conductive carbon particles, when LTO is cycled vs. high-potential cathode materials, is a direct proof of the cross-talk of organic-inorganic side reactions species formed at the cathode surface. Here, we focus on the cross-talk of the solvents by-products by following the local change at the C K-edge absorption acquired on conductive carbon particles, when LTO is cycled vs. Li-rich NCM and NCM111 cathodes. Figure 7a shows the C K-edge evolution on LTO cycled against Li-rich NCM in *Region 1* and *Region 2* (below 4.6 V), where the release of oxygen gas is only within the noise level, as reported by DEMS measurements.^[17] A similar trend is shown for the same regions for the stoichiometric NCM111 (Figure S13 in the Supplementary Information), where the O_2 evolution is, in this case, absent.^[17,30] Interestingly, we observe that, for both cathodes, the C K-edge remains free of any feature associated with EC or DMC by-product species, until 4.57 V. The only two detectable peaks are the unoccupied π^* and σ^* states of $\text{C}=\text{C}$ bond at 285.4 eV and 292.6 eV. Conversely, as expected, the LTO is covered by a surface layer caused by the reduction of the EC and DMC, noticeable by the components at 288.7 eV (carbonyl $\text{C}=\text{O}$) and 290.6 eV (carbonate CO_3^-), regardless of the cathode used (see Figure S14 in the Supplementary Information).^[34] The absence of carbon particles coverage is also shown from XPEEM compositional maps displayed in Figure 7b and 7c. The red areas, indicative of carbon particles, are not covered by a carbonate-layer (shown in yellow), which covers only areas occupied by the LTO particles (in blue).

Region 3 (after the O_2 release from the cathode): Following the same approach, we monitored the local C K-edge changes on carbon and LTO particles in *Region 3* above 4.8 V, after the release of O_2 gas from both the Li-rich and the stoichiometric NCM111 cathodes (Figure 8a and 8b). This time, we clearly see that the carbon particles are covered by carbonate species, through the components at 288.7 eV and 290 eV at the C K-edge, irrespective of whether the LTO electrode is cycled with the Li-rich or stoichiometric NCM111. These results strongly suggest that the O_2 gas, developed at the cathode surface, effectively contributes to the EC/DMC decomposition and initiates the electrolyte by-products cross-talk with the counter electrode. We can also notice that the less pronounced carbonate components intensity on LTO cycled vs. NCM111 is in line with the lower O_2 release from NCM111 (roughly 8 times lower than that developed from the Li-rich NCM).^[17] In order to follow the implication of the oxygen-triggered chemical

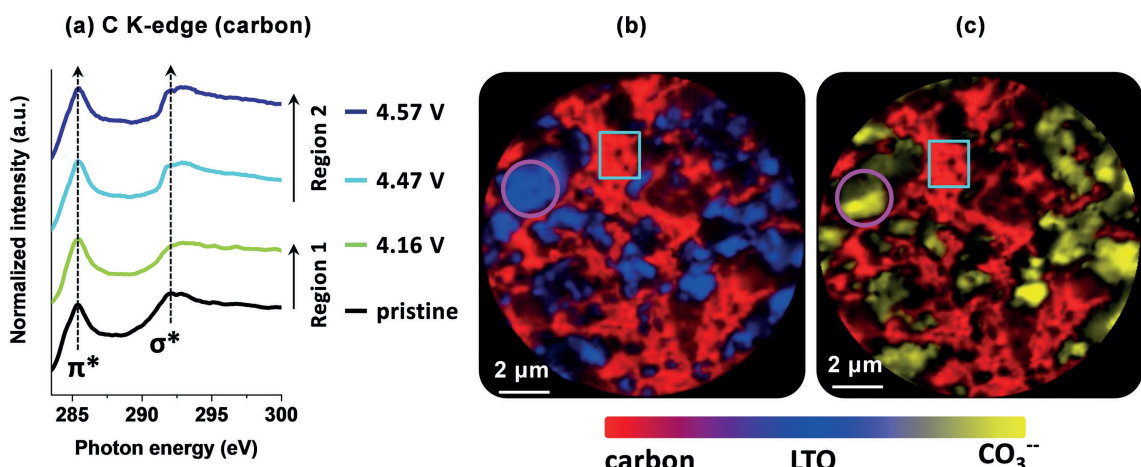


Figure 7. (a) Local XAS carried out at the C K-edge on carbon particles of LTO anodes cycled vs. Li-rich NCM. All spectra are taken for pristine (black curve) and cycled LTO anode along *Region 1* (green curve) and *Region 2* (cyan and blue curve). XPEEM compositional maps carried out at the (b) titanium L-edge in blue (458.3 eV) and carbon particles in red (285.6 eV) and on (c) carbonate in yellow (290.6 eV) to show the preferential coverage of the carbonate layer on the LTO particles.

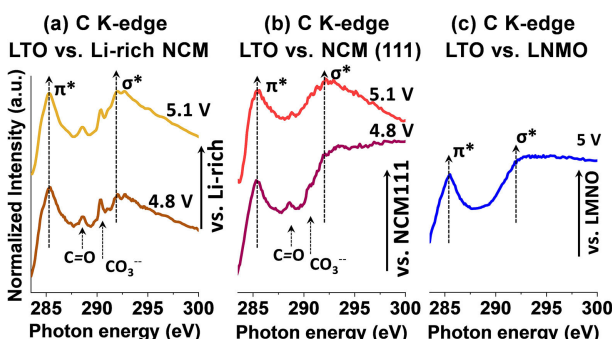


Figure 8. Local XAS carried out at the C K-edge on carbon particles of LTO anodes cycled vs. (a) Li-rich NCM, (b) NCM111 in *Region 3*, after the release of oxygen gas and (c) LNMO.

oxidation of the solvent and to exclude the contribution from a possible electrochemically-induced oxidation, we repeated the same experiment by cycling the LTO vs. LNMO to 5 V (Figure 8c). At this potential, the LNMO has almost no evolution of O₂, as reported by DEMS analysis^[14,24] and, accordingly, we do not observe carbonate coverage on carbon particles. These results support our hypothesis that the only electrolyte by-products components capable of migrating or diffusing to the LTO are those chemically decomposed by the oxygen released from the NCM-based cathodes rather than resulting from an electrochemical oxidation.

3. Discussion

In the first part of this work, we associated the oxygen loss from the Li-rich NCM cathode surface as the root-cause of the lower valence of the TMs and their subsequent dissolution into the electrolyte. When dissolution occurs, a “new and fresh” surface is created, which can explain the apparent oxidation of the TMs, as shown in the X-ray absorption spectra taken along

the charging process, especially at potential >4.47 V (in *Region 2*). Similarly, we also associated the TMs reduction observed at OCP to O loss from the surface, as a result of a chemical reaction with the electrolyte. To get more insight into the evolution of the oxygen loss, we calculate the ratio of the peak area at the O K-edge to the sum of Mn and Co L-edge peak areas (Figure 9), as a measure of the relative O to the TMs content at the particle surface. The oxygen peak area is calculated between 527 eV and 534 eV photon energy to avoid any possible contribution from Li₂CO₃ species from the surface. Interestingly, we observe a considerable decrease of the O/Mn+Co ratio at OCP, where it decreases to almost half of the value of the pristine electrode, after 54 days of soaking. Such decrease correlates with the detected reduced TMs layer of Mn^{2+/3+}, Co²⁺ and Ni²⁺ (Figure 2) and supports our hypothesis that O-surface instability (rather than Li⁺ loss) is the determining factor for the TMs lower valence. On the contrary, upon cycling, the O/Mn+Co ratio does not evolve considerably

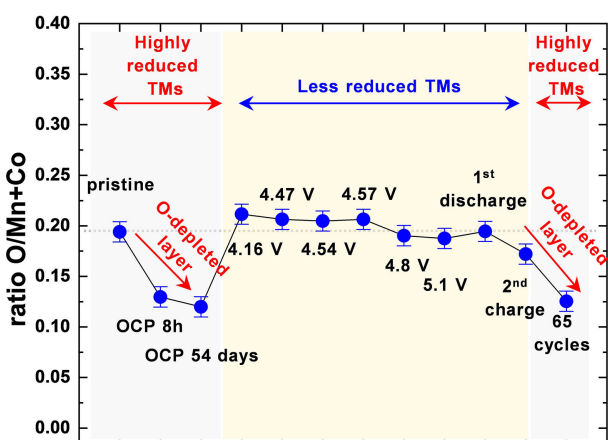


Figure 9. Oxygen evolution on the surface of the Li-rich NCM particles for pristine, stored at OCP and cycled cathodes as calculated from the areas of the O K-edge and Mn and Co L₃-edges.

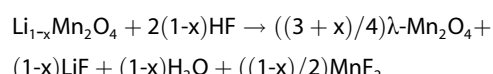
between 4.16 V and 4.57 V (*Region 1* and *Region 2*) as compared to the pristine state, in agreement with the little amount of reduced TMs. At the end of the charge, instead, at 4.8 V and 5.1 V, the ratio slightly drops, being again in line with the large amount of O release in this region, as discussed for the experiments shown in Figure 5. On 2nd charge and after long cycling (65 cycles) the ratio decreases further as for OCP conditions, implying a continual O loss and formation of reduced TMs over repeated cycling. The oxygen evolution on NCM111 reported in the supporting information (Figure S15) is also in line with the above observations and shows the absence of a depleted oxygen layer, except after long cycling, where the reduced TMs are more pronounced.

The origin of O loss and the presence of reduced TMs at OCP are strongly correlated to the oxygen reactivity at the interface between the layered oxide and the electrolyte. Indeed, as explained recently via DFT analysis, chemical oxidation of EC is thermodynamically favored on the LiMO₂ layered oxide and it is induced by the O lattice, via a dissociation mechanism that involves a proton transfer and reduction of the interfacial TMs ions.^[13,21] This mechanism can start already at OCP but becomes more favorable at a higher degree of delithiation. The EC dissociation is then followed by a series of reactions that leads to the formation of oligo-ether carbonates and polymers, predicted in theoretical reports^[20,35,36] and observed experimentally.^[23,37–41] A possible pathway for the EC dissociation follows the reaction proposed by Giordano *et al.*^[13]



where ${}^*\text{C}_3\text{O}_3\text{H}_3^+$ is the EC by-product adsorbed on the surface of the oxides (O–M–O). Such dissociation mechanism reduces the TMs from Mⁿ⁺ to M⁽ⁿ⁻¹⁾⁺ and produces a proton H⁺ that can either form an hydroxyl group on the oxide surface or react further with the electrolyte. Indeed, one of the immediate consequences is that the electrolyte acidity can increase, close to the interface, with the formation of HF^[42] in LiPF₆-containing electrolytes, well-known to accelerate further decomposition of both the electrolyte and the electrode components.^[17] Such reactions may explain the observed TMs reduction and their dissolution, both at OCP and for the cycled electrode.

Similar to the dissociation mechanism (which proceeds via a proton extraction), another oxidative decomposition can be initiated by the anion PF₆⁻, in a similar manner as for LiMn₂O₄.^[43]



On the other hand, the controversy concerning the migration or diffusion of the oxidized electrolyte solvent species (e.g. from EC and DMC) to the anode is elucidated here. We show that the only oxidized solvent by-products detected on the anode are the ones decomposed by the oxygen loss at the layered oxides through a chemical oxidation.

The chemical oxidation of the EC by the lattice oxygen (O²⁻) or oxygen radicals is also reported to form acyl fluoride species (ROCOF), carboxylate (HCO₂Li) and alkyl carbonate (ROCO₂Li).^[44] But it can also generate CO₂ gas and water as suggested by Jung *et al.*^[14] following the reaction:



Despite the aforementioned anodic chemical decomposition pathways, we detect no traces of oxidized by-products in the C K-edge spectra across the NCM cathode particles, neither at OCP nor upon cycling. This behavior is compatible with the scenario of dissolution into the electrolyte, caused by HF etching and/or by decomposition induced electrochemically at high potentials.

On the anode side instead, none of those solvent by-product species were detected until the cell reached the potential of the oxygen release from the cathode (4.8 V vs. Li⁺/Li). A plausible explanation is that, below 4.8 V, the by-products species concentration is not sufficiently high to be detected on the anode through the diffusion mechanism between the two electrodes. Alternatively, it can be argued that the by-products molecules formed below 4.8 V are neutrally charged and therefore are not subjected to the electric field force, which would drive their migration to the anode.

Besides the chemical reactions triggered by the O-species of the layered oxides or the salt by-products (i.e. HF), electrochemical oxidation of the electrolyte is still a likely degradation mechanism that we cannot fully disregard.^[38] Unfortunately, the discrimination between chemical and electrochemical processes is challenging, because they both form similar by-products in terms of electrolyte oligomers/polymers and gas compounds.^[23,44] However, even if it exists, the electrochemical oxidation of the solvents on the cathode does not lead to the migration or diffusion of the by-products to the anode, as shown by the absence of a surface layer on LTO cycled against the LNMO cathode at 5 V vs. Li⁺/Li.

Nonetheless, it is worth stressing that the surface layer that builds-up on LTO, caused by the migration or diffusion processes of oxidized solvents is relatively thin (less than 2 nm when using LiPF₆ salt). Of course, besides solvents by-products, there are other species, such as LiF and TMs, that are particularly abundant on the anode surface after long cycling and derive from the migration or diffusion of the oxidized LiPF₆ and PVDF from the cathode surface.^[28]

4. Conclusions

In this work, we examined in detail the role of the oxygen activity across the full-cell environment, by employing XPEEM as high resolution, surface-sensitive spectromicroscopy technique. On the surface of Li-rich NCM cathode we demonstrate the close synergy between oxygen and TMs redox activities. The latter are reduced to a lower valence as soon as oxygen loss occurs at the surface. Such process starts first without applying an electrochemical bias to the cell (i.e. at OCP)

through a chemical reaction between the electrolyte and the surface of the layered oxide. Then, it continues via an electrochemical reaction upon cycling at 4.47 V and is further enhanced at 4.8 V, when oxygen gas reaches a maximum release rate. The instability of the reduced TMs in contact with the electrolyte leads to their dissolution and deposition on the negative electrode. The loop related to the oxygen loss, transition metal reduction and dissolution makes the oxygen depleted layer very thin on the surface of the cathode particles even after long cycling. We also demonstrate that changing cathode stoichiometry to NCM111 does not alter such mechanism, except that it manifests to a smaller extent, due to the reduced oxygen release as compared to the Li-rich NCM. Simultaneously, we prove that the oxygen released at the cathode induces a chemical oxidation of the EC and DMC solvents with a formation of a carbonate layer that covers homogeneously the carbon and the active material of the counter electrode. The results on the LTO are indeed compelling in demonstrating that the cathode to anode cross-talk occurs only at 4.8 V, where the amount of O-induced by-products generated at the cathode surface is sufficiently high for their detection. By using the same approach, we attest unambiguously that the absence of oxygen release, as for LNMO, eliminates the chemical solvent oxidation and the related cross-talk with the LTO.

Experimental Section

Electrode Preparation and Cycling Conditions

Composite electrodes are prepared by casting a mixture of commercial active cathode materials of Li-rich $\text{Li}_{1.169}(\text{Ni}_{0.218}\text{Co}_{0.121}\text{Mn}_{0.661})_{0.83}\text{O}_2$ (Li-rich NCM), $\text{LiNi}_{0.33}\text{Co}_{0.33}\text{Mn}_{0.33}\text{O}_2$ (NCM111), $\text{LiNi}_{0.5}\text{Mn}_{1.5}\text{O}_4$ (LNMO) and anode material $\text{Li}_4\text{Ti}_5\text{O}_{12}$ (LTO), respectively, with polyvinylidene fluoride (PVDF Kynar HSV 900, Arkema) as organic binder, and Super-C carbon (Imerys) as conductive additive, in a mass ratio of 90:6:4 for the cathodes and 80:10:10 for LTO, all suspended in N-methyl-2-pyrrolidone (Fluka). The slurry is then spread onto an aluminum foil serving as current collector for both positive and negative electrodes. After drying the cast at 80°C overnight, circular 13 mm electrodes were punched out and pressed at 2 tons in order to reduce the surface roughness and porosity, which helped to improve the quality of the XPEEM images. Prior to cycling, both positive and negative electrodes were reheated at 120°C in a vacuum chamber at 10^{-2} mbar connected to an Ar-filled glovebox to remove any remaining water in the electrode. The electrodes were assembled in titanium-made coin-type cells using a glass fiber separator inserted between two Celgard 2400 separators, the latter to avoid silicate contamination at the surface of the electrodes. The electrolyte used consists of 1 M LiPF_6 solution in a mixture of 1:1 w/w of ethylene carbonate (EC) and dimethyl carbonate (DMC), called hereafter LP30 (BASF). The electrodes measured at open circuit potential (OCP) were soaked with the electrolyte either for 8 hours or 54 days inside the Ar-filled glovebox. The cathodes are cycled at a constant current (galvanostatic mode) vs. LTO using a 3-electrode cell configuration, with metallic lithium as reference. An OCP period of 6 hours is always applied before starting the cycling of the electrodes. For Li-rich NCM an average specific charge of 250 mAhg^{-1} is assumed and is cycled within the cut-off potential of 2.5–5.1 V vs. Li^+/Li , whereas for LTO a specific charge of 160 mAhg^{-1} is assumed and

the cycling is performed along its plateau at 1.55 V vs. Li^+/Li . Similar cycling is performed for the NCM111 cathode using cut-off potential limits of 2.5–4.8 V vs. Li^+/Li and assuming an average specific charge of 180 mAhg^{-1} . The LNMO is cycled instead between 3.0–5.0 V vs. Li^+/Li , considering an average specific charge of 150 mAhg^{-1} . All the experiments are conducted with a cycling rate of C/5 (five hours for discharge) and at room temperature (25°C). After cycling, the cells were disassembled in the glovebox, the electrodes gently washed by dipping the electrode in DMC solution to remove excess of salt and less volatile species like EC, then dried for 5 min in the Ar atmosphere of the glovebox. Then the electrodes were mounted on the XPEEM sample holders and finally transferred to the microscope under Ar with a transfer chamber specifically designed to avoid the detrimental air exposure. This sample preparation process is known to have a limited impact on the carbonate-rich layer as described by S. Malmgren et al.^[45]

X-ray Photoemission Electron Microscopy (XPEEM)

Imaging and X-ray absorption spectroscopy measurements are carried out at the SIM beamline installed at the Swiss Light Source (SLS), Paul Scherrer Institute (PSI), Switzerland. All the experiments are performed in ultra-high vacuum (5×10^{-10} mbar) at room temperature, by collecting secondary photoelectrons in partial electron yield with an energy resolution of 20 meV. To understand how the oxygen release can influence the stability of the cathode structure, we investigate the local electronic structure changes by following the XAS evolution on individual particles of the oxide material. The spatially-resolved XAS spectra obtained with XPEEM are carried out at the C, F and O K-edges and at the transition metals (TMs) L₃-edge for Mn, Co and Ni at OCP and upon cycling at different potentials along the first delithiation (Figure 1). X-ray PEEM elemental contrast images are obtained by pixel-wise division of two images recorded at the respective X-ray absorption edge and pre-edge. For example, for the Li-rich NCM electrodes the C K-edge is taken at 285.6 eV, the Mn L₃-edge at 641.6 eV and the F K-edge at 693 eV and their pre-edges energies are taken at 278 eV, 637 eV, and 683 eV, respectively. For LTO electrodes the same energies are used for the C and F K-edges, whereas for the Ti L₃-edge 458.3 eV and 454 eV are considered for the edge and pre-edge, respectively. For the lowest field of view used for the contrast images in our experiment (20 μm), a single pixel corresponds to ~40 nm, enabling us to analyze individual particles of Li-rich NCM and NCM111 (with a particle range of 2–10 μm), LTO (1–2 μm), LNMO (2–20 μm) and small cluster of conductive carbon (32 nm). The absorption spectra are obtained by recording a sequence of XPEEM images as a function of energy using linearly polarized light. Excepting for the C K-edge, all spectra are normalized by the incoming flux measured from a gold mesh or from the signal from a focusing mirror. For the analysis of the C K-edge, gold micro-particles deposited on the surface of pristine electrodes were used as a reference, in order to correct for the strong absorption at the carbon edge energies due to presence of carbon on the X-ray optics. From the contrast images one can choose a zone of interest on single particles from where the correspondent local absorption can be obtained from the XAS image sequence.

Acknowledgements

This work was performed at the Surfaces Interfaces: Microscopy (SIM) beamline at the Swiss Light Source (SLS), Paul Scherrer Institute (PSI), Villigen, Switzerland. The Swiss National Science Foundation and the PSI CROSS initiative are thanked for financial

support (Project 200021_156597). The manuscript was written through contributions of all authors. All authors have given approval to the final version of the manuscript.^[a,b] All authors contributed equally.

Conflict of Interest

The authors declare no conflict of interest.

Keywords: electrolyte stability • Li₄Ti₅O₁₂ anode • NCM-based cathodes • O₂ release • X-ray photoemission electron microscopy

- [1] S. Hy, H. Liu, M. Zhang, D. Qian, B. J. Hwang, Y. S. Meng, *Energy Environ. Sci.* **2016**, *9*, 1931–1954
- [2] A. R. Armstrong, M. Holzapfel, P. Novák, C. S. Johnson, S.-H. Kang, M. M. Thackeray, P. G. Bruce, *J. Am. Chem. Soc.* **2006**, *128*, 8694–8698
- [3] M. Sathiya, G. Rousse, K. Ramesha, C. P. Laisa, H. Vezin, M. T. Sougrati, M. L. Doublet, D. Foix, D. Gonbeau, W. Walker, *Nat. Mater.* **2013**, *12*, 827–835
- [4] E. McCalla, A. M. Abakumov, M. Saubanère, D. Foix, E. J. Berg, G. Rousse, M.-L. Doublet, D. Gonbeau, P. Novák, G. Van Tendeloo, *Science* **2015**, *350*, 1516–1521
- [5] M. Saubanère, E. McCalla, J. M. Tarascon, M. L. Doublet, *Energy Environ. Sci.* **2016**, *9*, 984–991
- [6] G. Assat, D. Foix, C. Delacourt, A. Iadecola, R. Dedryvère, J. M. Tarascon, *Nat. Commun.* **2017**, *8*, 2219
- [7] K. Luo, M. R. Roberts, R. Hao, N. Guerrini, D. M. Pickup, Y.-S. Liu, K. Edström, J. Guo, A. V. Chadwick, L. C. Duda, *Nat. Chem.* **2016**, *8*, 684–691
- [8] K. Luo, M. R. Roberts, N. Guerrini, N. Tapia-Ruiz, R. Hao, F. Massel, D. M. Pickup, S. Ramos, Y.-S. Liu, J. Guo, *J. Am. Chem. Soc.* **2016**, *138*, 11211–11218
- [9] W. E. Gent, K. Lim, Y. Liang, Q. Li, T. Barnes, A.-J. Ahn, K. H. Stone, M. McIntire, J. Hong, J. H. Song, *Nat. Commun.* **2017**, *8*, 2091
- [10] K. J. Carroll, D. Qian, C. Fell, S. Calvin, G. M. Veith, M. Chi, L. Baggetto, Y. S. Meng, *Phys. Chem. Chem. Phys.* **2013**, *15*, 11128–11138
- [11] A. Boulaineau, L. Simonin, J.-F. Colin, C. Bourbon, S. Patoux, *Nano Lett.* **2013**, *13*, 3857–3863
- [12] D. Qian, B. Xu, M. Chi, Y. S. Meng, *Phys. Chem. Chem. Phys.* **2014**, *16*, 14665–14668
- [13] L. Giordano, P. Karayaylali, Y. Yu, Y. Katayama, F. Maglia, S. Lux, Y. Shao-Horn, *J. Phys. Chem. Lett.* **2017**, *8*, 3881–3887
- [14] R. Jung, M. Metzger, F. Maglia, C. Stinner, H. A. Gasteiger, *J. Phys. Chem. Lett.* **2017**, *8*, 4820–4825
- [15] B. Strehle, K. Kleiner, R. Jung, F. Chesneau, M. Mendez, H. A. Gasteiger, M. Piana, *J. Electrochem. Soc.* **2017**, *164*, A400–A406
- [16] E. Castel, E. J. Berg, M. El Kazzi, P. Novák, C. Villevieille, *Chem. Mater.* **2014**, *26*, 5051–5057
- [17] A. Guéguen, D. Streicher, M. He, M. Mendez, F. F. Chesneau, P. Novák, E. J. Berg, *J. Electrochem. Soc.* **2016**, *163*, A1095–A1100
- [18] D. Streicher, C. Erk, A. Guéguen, P. Müller, F.-F. Chesneau, E. J. Berg, *J. Phys. Chem. C* **2017**, *121*, 13481–13486
- [19] S. E. Renfrew, B. D. McCloskey, *J. Am. Chem. Soc.* **2017**, *139*, 17853–17860
- [20] O. Borodin, W. Behl, T. R. Jow, *J. Phys. Chem. C* **2013**, *117*, 8661–8682
- [21] M. Gauthier, T. J. Carney, A. Grimaud, L. Giordano, N. Pour, H.-H. Chang, D. P. Fenning, S. F. Lux, O. Paschos, C. Bauer, *J. Phys. Chem. Lett.* **2015**, *6*, 4653–4672
- [22] K. Xu, S. P. Ding, T. R. Jow, *J. Electrochem. Soc.* **1999**, *146*, 4172–4178
- [23] M. Moshkovich, M. Cojocaru, H. E. Gottlieb, D. Aurbach, *J. Electroanal. Chem.* **2001**, *497*, 84–96
- [24] M. He, L. Boulet-Roblin, P. Borel, C. Tessier, P. Novák, C. Villevieille, E. J. Berg, *J. Electrochem. Soc.* **2016**, *163*, A83–A89
- [25] H. Koga, L. Croguennec, M. Ménétrier, P. Mannessiez, F. Weill, C. Delmas, S. Belin, *J. Phys. Chem. C* **2014**, *118*, 5700–5709
- [26] F. Lin, D. Nordlund, I. M. Markus, T.-C. Weng, H. L. Xin, M. M. Doeff, *Energy Environ. Sci.* **2014**, *7*, 3077–3085
- [27] F. Lin, I. M. Markus, D. Nordlund, T.-C. Weng, M. D. Asta, H. L. Xin, M. M. Doeff, *Nat. Commun.* **2014**, *5*, 3529
- [28] D. Leanza, C. A. F. Vaz, G. Melinte, X. Mu, P. Novák, M. El Kazzi, *ACS Appl. Mater. Interfaces* **2018**, *11*, 6054–6065
- [29] C. Tian, D. Nordlund, H. L. Xin, Y. Xu, Y. Liu, D. Sokaras, F. Lin, M. M. Doeff, *J. Electrochem. Soc.* **2018**, *165*, A696–A704
- [30] R. Jung, M. Metzger, F. Maglia, C. Stinner, H. A. Gasteiger, *J. Electrochem. Soc.* **2017**, *164*, A1361–A1377
- [31] B. J. Hwang, Y. W. Tsai, D. Carlier, G. Ceder, *Chem. Mater.* **2003**, *15*, 3676–3682
- [32] J. Xu, M. Sun, R. Qiao, S. E. Renfrew, L. Ma, T. Wu, S. Hwang, D. Nordlund, D. Su, K. Amine, *Nat. Commun.* **2018**, *9*, 947
- [33] D. Streicher, A. Guéguen, M. Mendez, F. Chesneau, P. Novák, E. J. Berg, *J. Electrochem. Soc.* **2016**, *163*, A964–A970
- [34] D. Leanza, C. A. F. Vaz, I. Czekaj, P. Novák, M. El Kazzi, *J. Mater. Chem. A* **2018**, *6*, 3534–3542
- [35] L. Xing, O. Borodin, *Phys. Chem. Chem. Phys.* **2012**, *14*, 12838–12843
- [36] X. Zhang, J. K. Pugh, P. N. Ross, *J. Electrochem. Soc.* **2001**, *148*, E183–E188
- [37] B. Vortmann, S. Nowak, C. Engelhard, *Anal. Chem.* **2013**, *85*, 3433–3438
- [38] M. Metzger, C. Marino, J. Sicklinger, D. Haering, H. A. Gasteiger, *J. Electrochem. Soc.* **2015**, *162*, A1123–A1134
- [39] D. Aurbach, K. Gamolsky, B. Markovsky, G. Salitra, Y. Gofer, U. Heider, R. Oesten, M. Schmidt, *J. Electrochem. Soc.* **2000**, *147*, 1322–1331
- [40] S. E. Sloop, J. B. Kerr, K. Kinoshita, *J. Power Sources* **2003**, *119*–121, 330–337
- [41] P. Niehoff, M. Winter, *Langmuir* **2013**, *29*, 15813–15821
- [42] R. Dedryvère, H. Martinez, S. Leroy, D. Lemordant, F. Bonhomme, P. Biensan, D. Gonbeau, *J. Power Sources* **2007**, *174*, 462–468
- [43] M. Wohlfahrt-Mehrens, C. Vogler, J. Garche, *J. Power Sources* **2004**, *127*, 58–64
- [44] M. A. Teshager, S. D. Lin, B.-J. Hwang, F.-M. Wang, S. Hy, A. M. Haregewoin, *ChemElectroChem* **2016**, *3*, 337–345
- [45] S. Malmgren, K. Ciosek, R. Lindblad, S. Plogmaker, J. Kühn, H. Rensmo, K. Edström, M. Hahlin, *Electrochim. Acta* **2013**, *105*, 83–91

Manuscript received: November 15, 2018

Revised manuscript received: February 22, 2019

Accepted manuscript online: February 25, 2019

Version of record online: March 25, 2019